Journal of Luminescence 134 (2013) 594–599

Contents lists available at SciVerse ScienceDirect

Journal of Luminescence

journal homepage: www.elsevier.com/locate/jlumin

Linear and nonlinear optical absorption coefficients in GaAs/$Ga_{1-x}Al_xAs$ concentric double quantum rings: Effects of hydrostatic pressure and aluminum concentration

H.M. Baghramyan [a], M.G. Barseghyan [a,*], A.A. Kirakosyan [a], R.L. Restrepo [b], C.A. Duque [c]

[a] Department of Solid State Physics, Yerevan State University, Al. Manookian 1, 0025 Yerevan, Armenia
[b] Escuela de Ingeniería de Antioquia, AA 7516 Medellín, Colombia
[c] Instituto de Física, Universidad de Antioquia, AA 1226 Medellín, Colombia

ARTICLE INFO

Article history:
Received 9 May 2012
Received in revised form
3 July 2012
Accepted 25 July 2012
Available online 2 August 2012

Keywords:
Quantum ring
Hydrostatic pressure
Nonlinear optical properties

ABSTRACT

The linear and nonlinear intra-band optical absorption coefficients in GaAs/$Ga_{1-x}Al_xAs$ two-dimensional concentric double quantum rings are investigated. Taking into account the combined effects of hydrostatic pressure and aluminum concentration the energies of the ground ($n=1$, $l=0$) and the first excited state ($n=2$, $l=1$) have been found using the effective mass approximation and the transfer matrix formalism. The energies of these states and the corresponding threshold energy of the intra-band optical transitions are examined as a function of hydrostatic pressure and aluminum concentration for different sizes of the structure. We also investigated the dependencies of the linear, nonlinear, and total optical absorption coefficients as functions of the incident photon energy for different values of hydrostatic pressure, aluminum concentration, sizes of the structure, and incident optical intensity. Its is found that the effects of the hydrostatic pressure and the aluminum concentration lead to a shifting of the resonant peaks of the intra-band optical spectrum.

1. Introduction

Electron-related exchange and correlation effects, Coulomb interaction between electron and hole carriers, as well as confinement and strain effects in quantum dots (QD) are subjects of great interest in condensed matter physics. In all of them, quantum properties are expected to play a vital role in bringing out possible special features. Since these QDs possess discrete energy levels, they may exhibit novel physical phenomena which are entirely different from their bulk materials. Changing the shape and size of these dots provides great advantages in view of tuning desired properties. Theoretical studies on vertically coupled QDs have been put forward in recent times [1–7]. In Refs. [1,2] the electron, hole, and exciton spectra in the strained QD molecule consisting of three vertically arranged type-II InP/$In_{0.49}Ga_{0.51}P$ self-assembled QDs are modeled by the $\mathbf{k}\cdot\mathbf{p}$ theory. The exciton states are obtained from an exact diagonalization method, and the authors also compute the oscillator strength for recombination processes. The properties of excitons confined in a type-II QD under the influence of perpendicular applied magnetic field are studied in Ref. [4]. The Stark effect on exciton states in single and vertically coupled type-I and type-II QDs has been investigated by Janssens et al. [5]. Kuskovsky and co-workers [6] studied excitons in vertically stacked type-II QDs finding that this system shows a topological magnetic phase; also they demonstrate the presence of Aharonov–Bohm oscillations in the emission intensity. In the same work, the photoluminescence of vertically stacked ZnTe/ZnSe QDs is measured in magnetic fields up to 31 T. In their study the positions of the peaks of the emission intensity are in good agreement with numerical simulations of excitons in stacked QDs. On the other hand, the work by Mora-Ramos et al. considers the effects of the hydrostatic pressure and applied magnetic field on the exciton properties of GaAs–(Ga,Al)As QDs.

Since the first quantum rings (QRs) of nanoscopic sizes were fabricated [8,9], these fascinating systems have drawn a considerable attention due to the interest in studying physical phenomena such as the Aharonov–Bohm effect [10–13] and the appearance of persistent currents [14]. Theoretical studies on vertically [15–18] and laterally [19,20] coupled double QRs have discussed the molecular properties of these systems. QRs may also be coupled concentrically. In Refs. [21,22] the authors demonstrated the self-assembled formation of GaAs concentric double quantum rings (CDQRs) with high uniformity and excellent rotational symmetry using the droplet epitaxy technique. When compared with single QRs, these ring complexes open a new promising route, foreseen

* Corresponding author. Tel.: +374 504505.
E-mail address: mbarsegh@ysu.am (M.G. Barseghyan).

0022-2313/$ - see front matter © 2012 Elsevier B.V. All rights reserved.
http://dx.doi.org/10.1016/j.jlumin.2012.07.024

by the use of novel ring geometries, to the measurement of quantum interference effects [23,24]. A series of recent works have addressed their electronic properties [25–30] and far-infrared response [31,32]. It has been shown for example that the energy spectrum of a system of two concentric coupled rings, with similar confinement length, corresponds roughly to the superposition of the spectra of two independent rings, although interesting anti-crossings among different states of the individual rings – with the same angular momentum – can be observed [26]. Culchac et al. [33] have investigated the influence of axial magnetic field and geometric confinement on the electronic states in two-dimensional CDQRs, finding an interesting behavior of the probability amplitude of the electron state that reflects the competition between geometric and magnetic confinements. Electronic tunneling between the coupled rings may be reinforced or suppressed by conveniently modulating the barrier size separating the two rings, leading to a drastic change in the electronic charge distribution through the nanostructure. In Ref. [34], two concentric two-dimensional GaAs/(Al,Ga)As QRs in a normal magnetic field are theoretically studied. The single-band effective mass approximation is adopted for both the electron and the hole states, and the analytical solutions are given. The authors have shown that the oscillator strength for inter-band transitions is strongly reduced close to each anti-crossing and also that the optical excitonic Aharonov–Bohm effect may occur in QRs.

The influences of hydrostatic pressure and magnetic field on the ground and excited electron states and on the electron–heavy hole energy transitions in GaAs/$Ga_{1-x}Al_xAs$ CDQRs have been investigated by Culchac and co-workers [35]. For both, symmetric and antisymmetric CDQRs, it is found that the electron–heavy hole energy transition augments with the hydrostatic pressure, which is mainly due to the pressure-induced increase in the GaAs bandgap. Taking into account the combined effects of electric field, hydrostatic pressure, temperature, and aluminum concentration, the ground state energy of an electron in GaAs/$Ga_{1-x}Al_xAs$ CDQRs is calculated by Baghramyan et al. [36,37]. The ground state energy dependencies on the mentioned factors have been reported for different values of the sizes of the rings. The authors found that the considered effects mainly depend on the dimensions of the QRs.

The nonlinear optical properties, such as optical absorption [38,39], have shown high potential for device applications in far-infrared laser amplifiers [40], photo-detectors [41], and high speed electro-optical modulators [42]. Therefore, for both fundamental and applied researches, the nonlinear optical properties of semiconductor quantum heterostructures have attracted much attention in recent years [43–48]. The effects of asymmetry and applied electric field on the electronic subbands and the nonlinear intersubband optical absorption in GaAs quantum wells with Pöschl–Teller confining potential have been studied by Yildirim and Tomak [43]. Karabulut and Baskoutas [44] have investigated the effects of shallow-impurities, external applied electric field, and intensity of the incident radiation on the optical properties of spherical QDs with parabolic confinement. The results showed that with the increase of the electric field, and/or the electron-impurity distance, and/or the QD radius, there will be induced blueshift and/or redshift of the peak positions of the total absorption coefficient. The effect of impurities on the linear and nonlinear optical absorption in a disc-like parabolic QD has been performed by Xie [45]. The author has shown that the total optical absorption coefficient is strongly affected by the incident optical intensity and the confinement strength. Using exact diagonalization techniques, the low-lying states of an exciton and the linear and nonlinear optical absorptions in a disc-like QD are theoretically studied by Yuan and co-workers [46]. Their results show that the total optical absorption coefficient is about two times bigger than the corresponding one obtained without considering the exciton effects. Additionally, they found that the optical absorption saturation intensity can be controlled by the incident optical intensity. The linear and nonlinear optical absorption coefficients have been calculated in single QR taking into account the electron–electron interaction in Ref. [47]. The author reports that the intersubband optical absorption strongly depends on the QR radius, electron–electron interaction, and the incident optical intensity. The effects of exciton and magnetic field on the linear and nonlinear optical absorption in a single QR has investigated in Ref. [48]. Their results show the possibility to control the properties of nonlinear optical absorption of a QR by tuning the outer and inner radius. Moreover, the authors have found that the nonlinear optical properties of a QR can be modulated by the magnetic flux through the QR. Also, there are recent reports on the influence of hydrostatic pressure on the nonlinear optical properties of GaAs-based quantum nanostructures (see, for instance, Refs. [49,50]).

In the present work the effects of hydrostatic pressure, aluminum concentration, and sizes of the structure on the linear and the nonlinear intra-band optical transitions in GaAs/$Ga_{1-x}Al_xAs$ two-dimensional CDQR are investigated. The paper is organized as follows. In Section 2 we describe the theoretical framework. Section 3 is dedicated to the results and discussion, and our conclusions are given in Section 4.

2. Theoretical framework

Fig. 1 presents a pictorial view of the CDQR geometry considered in this work. The dimensions of the heterostructure (radii, widths, and the thickness of rings) are depicted there. Usually the thickness of the ring is smaller than the radial dimensions. So, our system can be considered as a two-dimensional one with the electron confined in the plane $z=0$ ($H\to 0$).

The radial sizes of the structure depend on the hydrostatic pressure (P) according to the expression [35,51,52]

$$\rho(P)=\rho(0)[1-2(S_{11}+2S_{12})P]^{1/2}, \quad (1)$$

where S_{11} and S_{12} are the components of the compliance tensor of GaAs ($S_{11}=1.16\times10^{-3}$ kbar^{-1} and $S_{12}=-3.7\times10^{-4}$ kbar^{-1}).

The Hamiltonian of the electron in a CDQR in the effective mass and parabolic band approximations, under the effects of hydrostatic pressure, temperature, and for aluminum concentration x is

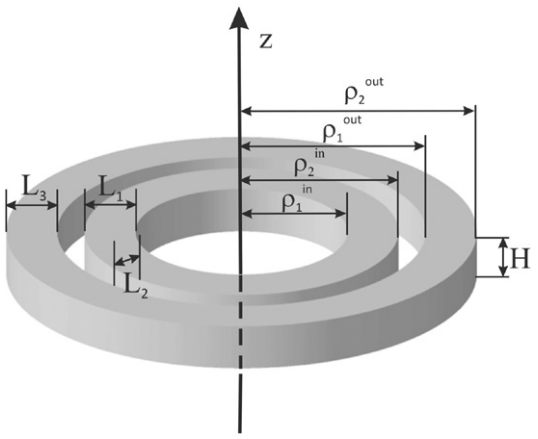

Fig. 1. The CDQR heterostructure: L_1 is the width of the inner ring, L_2 is the width of the coupling barrier, L_3 is the width of the outer ring, ρ_1^{in} and ρ_2^{in} are the inner and outer radii of the inner ring; ρ_1^{out} and ρ_2^{out} are the inner and outer radii of the outer ring, and H is the thickness of rings.

given by Ref. [37]

$$\hat{H}_{\rho\varphi} = -\frac{\hbar^2}{2}\left[\frac{1}{\rho}\frac{\partial}{\partial\rho}\left(\frac{\rho}{m(x,P,T)}\frac{\partial}{\partial\rho}\right)+\frac{1}{m(x,P,T)}\frac{1}{\rho^2}\frac{\partial^2}{\partial\varphi^2}\right]+V(\rho,x,P,T), \tag{2}$$

where $m(x,P,T)$ is the aluminum concentration, temperature ($T=4$ K in this work), and hydrostatic pressure dependent electron effective mass, which is given by Ref. [53]

$$m(x,P,T) = m_0\left[1+\frac{\Pi^2(x)}{3}\left(\frac{2}{E_g^{\Gamma}(x,P,T)}+\frac{1}{E_g^{\Gamma}(x,P,T)+\Delta_0(x)}\right)+\delta(x)\right]^{-1}. \tag{3}$$

Here m_0 is the free electron mass, $\Pi(x)$ is the inter-band matrix element [$\Pi^2(x) = (28\,900-6290x)$ meV] and $\Delta_0(x)$ is the valence-band spin–orbit splitting [$\Delta_0(x) = (341-66x)$ meV]. The remote-band effects are taken into account via the $\delta(x)$ parameter, which is given by the expression $\delta(x) = -3.935+0.488x+4.938x^2$.

On the other hand, the energy gap function at the i-point ($i=\Gamma$,X) of the conduction band is given by the expression

$$E_g^i(x,P,T) = a_i+b_ix+c_ix^2+\alpha_iP-\frac{\beta_iT^2}{\gamma_i+T}, \tag{4}$$

where the values of parameters a_i, b_i, c_i, α_i, β_i, and γ_i are given in Table 1. They have been taken from photoluminescence measurements [53].

The confining potentials are defined taking into account the hydrostatic pressure induced crossover between the Γ and X minima of the conduction band [37,53,54]. Then, with the inclusion of the crossover effect the confining potential is given by

$$V(\rho,x,P,T) = \begin{cases} 0 & \text{if } \rho_1^{in}\le\rho\le\rho_2^{in} \text{ and } \rho_1^{out}\le\rho\le\rho_2^{out}, \\ V(x,P,T) & \text{if } \rho<\rho_1^{in},\rho_2^{in}<\rho<\rho_1^{out} \text{ and } \rho>\rho_2^{out}, \end{cases} \tag{5}$$

where

$$V(x,P,T) = r\begin{cases} E_g^{\Gamma}(x,P,T)-E_g^{\Gamma}(0,P,T) & \text{if } P\le P_1(x,T), \\ E_g^{X}(x,P,T)-E_g^{\Gamma}(0,P,T)+S_{\Gamma X}(x,P,T) & \text{if } P_1(x,T)<P\le P_2(x,T). \end{cases} \tag{6}$$

Here, r is the fraction of band gap discontinuity associated with the confinement potential for electrons, $P_1(x,T)$ is the critical value of the hydrostatic pressure at which the crossover between the Γ and X bands at the $Ga_{1-x}Al_xAs$ barrier occurs, and $P_2(x,T)$ corresponds to the crossover between the Γ-band at the GaAs well and the X-band at the $Ga_{1-x}Al_xAs$ barrier.

The eigenfunctions of the Hamiltonian in Eq. (2) can be presented in the form $\Phi(\rho,\varphi) = Ne^{il\varphi}f_{n,l}(\rho)$, where N is the normalization constant, and $n=1,2,\ldots$, and $l=0,\pm1,\pm2,\ldots$ are the quantum numbers. The $f_{n,l}(\rho)$ eigenfunctions, with eigenvalues $E_{n,l}$, are obtained from a suitable linear combination of Bessel functions. In order to find the $E_{n,l}$ energies and the corresponding wavefunctions, the transfer matrix formalism is used [55].

Using the density matrix approach, the linear and third order optical absorption coefficients can be written, respectively, as [39,56]

$$\alpha^{(1)}(\hbar\omega) = \frac{4\pi\omega}{\varepsilon(P,T)^{1/2}c}\frac{\sigma_s|M_{fi}|^2\Gamma_0}{(E_{fi}-\hbar\omega)^2+\Gamma_0^2} \tag{7}$$

and

$$\alpha^{(3)}(\hbar\omega,I) = -\frac{32\pi^2\omega}{\varepsilon(P,T)c^2}\frac{I\sigma_s|M_{fi}|^4\Gamma_0}{[(E_{fi}-\hbar\omega)^2+\Gamma_0^2]^2} \times\left[1-\left|\frac{M_{ff}-M_{ii}}{2M_{fi}}\right|^2\frac{(E_{fi}-\hbar\omega)^2-(\Gamma_0)^2+2E_{fi}(E_{fi}-\hbar\omega)}{E_{fi}^2+\Gamma_0^2}\right], \tag{8}$$

where Γ_0 ($=0.4$ meV) is the Lorentzian – damping-related – parameter, $\varepsilon(P,T)$ is the pressure and temperature dependent GaAs static dielectric constant, which for $T\le200$ K is given by

$$\varepsilon(P,T) = 12.74\exp[-16.7\times10^{-4}P+9.4\times10^{-5}(T-75.6)]. \tag{9}$$

In Eqs. (7) and (8), I represents the intensity of the incident field, σ_s ($=3\times10^{16}$ cm^{-3}) is the density of the electrons, $E_{fi}=E_f-E_i$, and $M_{fi} = \langle n',l'|e\rho\cos(\varphi)|n,l\rangle = \langle2,1|e\rho\cos(\varphi)|1,0\rangle$ is the matrix element of the dipole operator, with e the electron charge. In this case the selection rules for the matrix element of the dipole operator indicate that the transitions are allowed for $\Delta l = \pm1$.

Table 1

Γ-minimum	X-minimum
$a_\Gamma = 1519.4$ meV	$a_X = 198$ meV
$b_\Gamma = 1360$ meV	$b_X = 207$ meV
$c_\Gamma = 220$ meV	$c_X = 55$ meV
$\alpha_\Gamma = 10.7$ meV/kbar	$\alpha_X = -1.35$ meV/kbar
$\beta_\Gamma = 0.5405$ meV/K	$\beta_X = 0.46$ meV/K
$\gamma_\Gamma = 204$ K	$\gamma_X = 204$ K

3. Results and discussion

In Fig. 2(a) and (b) the dependencies on the hydrostatic pressure of the ground ($n=1$, $l=0$) and first excited ($n=2$, $l=1$) state energies are shown for different values of the widths of the outer ring L_3 and coupling barrier L_2. From the figures we may observe that both energies are decreasing functions of pressure. Such a behavior can be explained as follows. For $P\le P_1$ the radial-confining potential height is constant and the energy decrease is only due to the increase of the electron effective mass with pressure. If $P_1<P<P_2$ there will be a faster decrease in the electron energy with pressure; because in addition to the decrease associated to the growth in the value of the electron effective mass, now there is an extra reduction in the energy. This is associated with the fall in the radial-potential barrier height. Here, one may notice that the energy decreases with the increase of L_3 as a result of the weakening of the size quantization. Also, by comparing the corresponding curves in Fig. 2(a) and (b), we

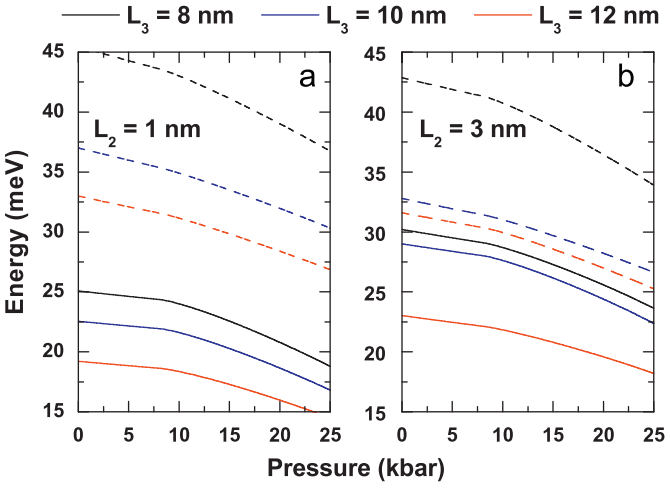

Fig. 2. Electron energy as a function of the hydrostatic pressure: solid lines are for the ground state whereas the dashed lines are for the first excited state. The results are for $x=0.3$, $L_1=10$ nm with $L_2=1$ nm (a) and with $L_2=3$ nm (b). Several values of the width of the outer ring L_3 have been investigated.

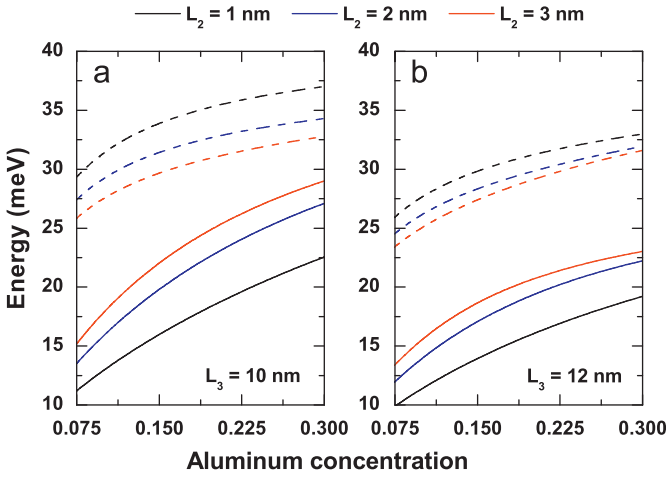

Fig. 3. Electron energy as a function of the aluminum concentration: solid lines are for the ground state whereas the dashed lines are for the first excited state. The results are for $P=0$, $L_1=10$ nm with $L_3=10$ nm (a) and with $L_3=12$ nm (b). Different values of the width of the coupling barrier L_2 have been investigated.

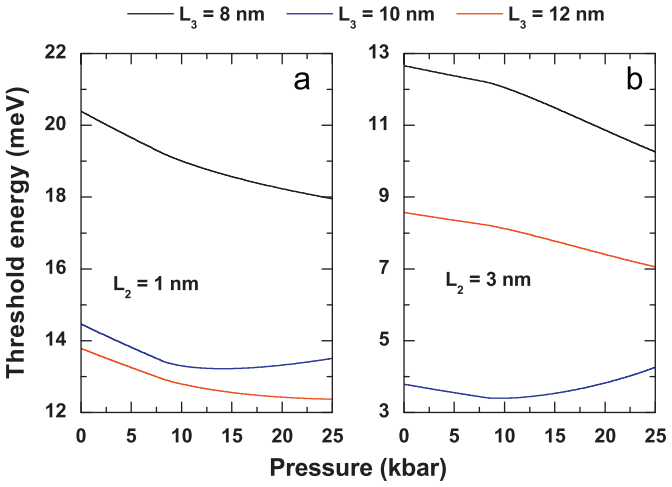

Fig. 4. Threshold energy of the intra-band optical transition between the ground and the first excited state as a function of the hydrostatic pressure. The results are for $x=0.3$, $L_1=10$ nm with $L_2=1$ nm (a) and with $L_2=3$ nm (b). Different values of the width of the outer ring L_3 have been investigated.

observe that the energy of the ground and the excited states are decreasing functions of the size of the coupling barrier as well. This is a consequence of the fact that with the increasing of the coupling barrier width the overlapping between the states in the inner and the outer rings becomes smaller, and the energy of each state reflects its tendency towards the more stable condition, which is independent of any further increasing of the coupling barrier width.

The ground and first excited state energies as functions of the aluminum concentration for several values of the coupling barrier width are presented in Fig. 3. Here we can see the same increasing behavior of the ground and the first excited state in regard with the increment in the coupling barrier width, as well as the decreasing behavior of the distance between the energy levels of the mentioned states if the system goes from the symmetric ($L_3=10$ nm) to the asymmetric ($L_3=12$ nm) structure geometries. We observe also the evolution of the energy as an increasing function of x, given the corresponding strengthening of the radial-confining potential for larger barrier heights (although the effective mass in the barrier region is larger as well, thus inducing an energy decrease, the influence of the variation of the confining potential height is stronger and clearly dominates). We also notice the strong influence of the x-variation on the dependence of the energy on L_2 which is the combined result of the increasing of the effective mass in the barrier region and increasing of the radial confining potential height.

Fig. 4(a) and (b) contains the threshold energy ($E_{2,1}-E_{1,0}$) associated with the transition between the ground state ($n=1$, $l=0$) and the first excited state ($n=2$, $l=1$) varying as a function of hydrostatic pressure, for different values of the width of the outer ring L_3. We can see that the threshold energy is a decreasing function of the pressure for $L_3=8$ nm and $L_3=12$ nm but it has both decreasing and increasing behaviors in the case $L_3=10$ nm. This is associated with the change in the rate of decreasing of the ground and first-excited state energies, which can be seen in Fig. 2. It is also observed a different behavior of the threshold energy as a function of L_3 in both $L_2=1$ nm and $L_2=3$ nm cases, which can also be understood from the energy spectrum shown in Fig. 2.

In Fig. 5 we depict the variation of the threshold energy resulting from the change in the aluminum concentration, for several values of L_2. It can be seen that the threshold energy decreases with the increase of L_2 and that its dependence on x has a strong influence of variation of L_2: in Fig. 5(a) the threshold

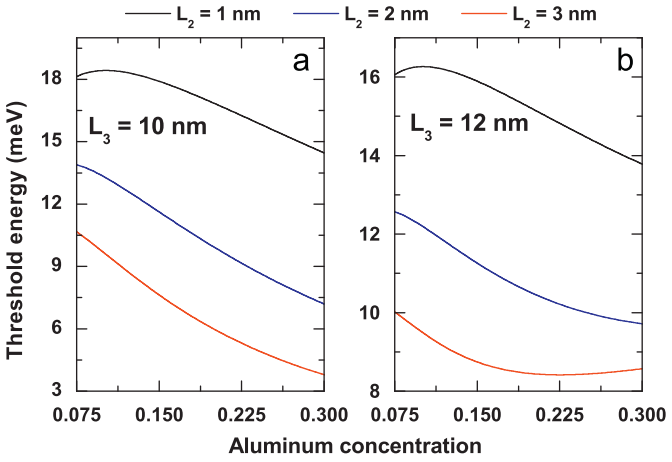

Fig. 5. Threshold energy of the intra-band optical transition between the ground and first excited state as a function of the aluminum concentration. The results are for $P=0$, $L_1=10$ nm with $L_3=10$ nm (a) and with $L_3=12$ nm (b). Different values of the width of the coupling barrier L_2 have been investigated.

energy is a decreasing function of x for $L_2=2$ nm and $L_2=3$ nm but changes its behavior type for $L_2=1$ nm near the $x=0.1$ point and the same behavior we see in Fig. 5(b). All these variations of threshold energy can be understood from the energy dependencies on x in Fig. 3.

In Fig. 6 the linear, nonlinear, and total absorption coefficients are shown as functions of the energy of the incident photon for several values of hydrostatic pressure. A redshift is observed if we go from $P=0$ to $P=15$ kbar whereas a blueshift appears in the region from $P=15$ kbar to 25 kbar. This happens because, with the increase of the hydrostatic pressure, the threshold energy of intra-band transition [Fig. 4(a)] decreases for low pressures and then augments when P becomes larger.

Fig. 7 depicts the linear, nonlinear and total absorption coefficients as functions of the incident photon energy for several values of the coupling barrier width L_2. From the figure, it is possible to observe the redshift of the absorption coefficients with L_2, in agreement with Fig. 5(a).

Moreover, in Fig. 8 we are presenting the variations of the linear, nonlinear and total absorption coefficients as functions of the energy of the incident photon for different values of the aluminum concentration. Here it can be observed that there is a

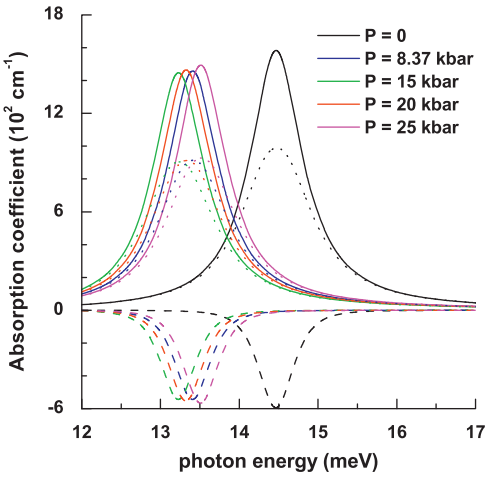

Fig. 6. Absorption coefficient as a function of the energy of the incident photon: solid lines are for $\alpha_1(\hbar\omega)$, dashed lines are for $\alpha_3(\hbar\omega,I)$, and dotted lines are for $\alpha(\hbar\omega,I)=\alpha_1(\hbar\omega)+\alpha_3(\hbar\omega,I)$. The results are for $L_1=10$ nm, $L_2=1$ nm, $L_3=10$ nm, $x=0.3$, and $I=5\times10^3$ W/cm^2. Different values of hydrostatic pressure have been investigated.

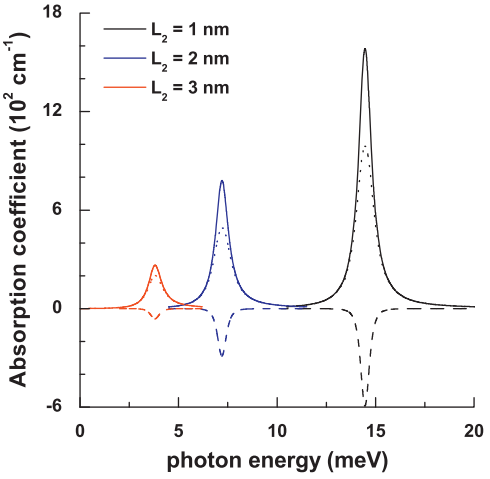

Fig. 7. Absorption coefficient as a function of the energy of the incident photon: solid lines are for $\alpha_1(\hbar\omega)$, dashed lines are for $\alpha_3(\hbar\omega,I)$, and dotted lines are for $\alpha(\hbar\omega,I)=\alpha_1(\hbar\omega)+\alpha_3(\hbar\omega,I)$. The results are for $P=0$, $L_1=10$ nm, $L_3=10$ nm, $x=0.3$, and $I=5\times10^3$ W/cm^2. Different values of the width of the coupling barrier L_2 have been investigated.

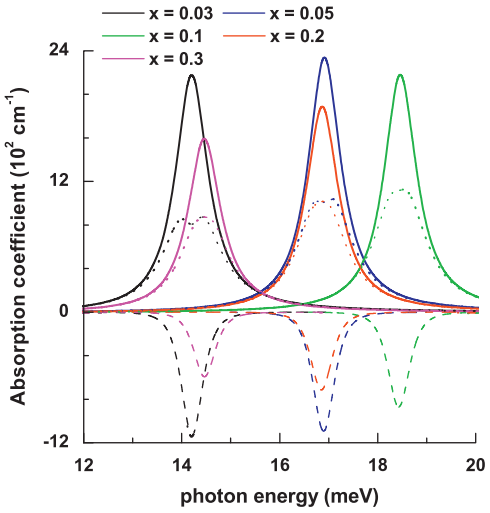

Fig. 8. Absorption coefficient as a function of the energy of the incident photon: solid lines are for $\alpha_1(\hbar\omega)$, dashed lines are for $\alpha_3(\hbar\omega,I)$, and dotted lines are for $\alpha(\hbar\omega,I)=\alpha_1(\hbar\omega)+\alpha_3(\hbar\omega,I)$. The results are for $P=0$, $L_1=10$ nm, $L_2=1$ nm, $L_3=10$ nm and $I=6\times10^3$ W/cm^2. Different values of aluminum concentration x have been investigated.

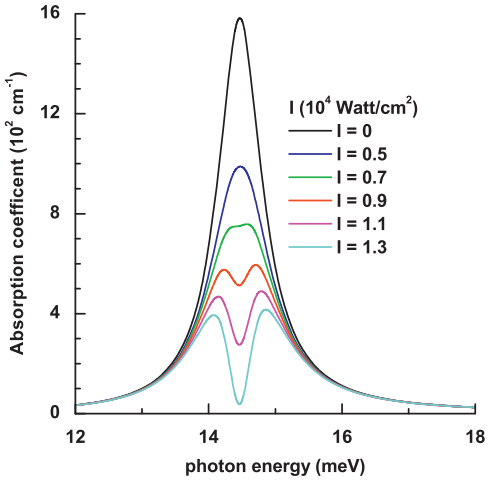

Fig. 9. Total absorption coefficient as a function of the incident photon energy. The results are for $P=0$, $L_1=10$ nm, $L_2=1$ nm, $L_3=10$ nm, and $x=0.3$. Different values of the incident optical intensity have been investigated.

blueshift when the aluminum concentration goes from $x=0.03$ to $x=0.1$, whilst the appearance of a redshift becomes apparent when this parameter changes from $x=0.1$ to $x=0.3$, in agreement with what it is shown in Fig. 5(a). Besides that, we see that the total absorption coefficient splits up into two peaks, which is the consequence of the bleached absorption (in smaller values of x the distance between energy levels is smaller which leads to the decreasing of the linear absorption coefficient in such a way that, with the appropriate choice of the incident optical intensity, the influence of the third order coefficient can lead to this splitting).

As it can be readily seen in all figures containing optical absorption results, there is no strong monotonic behavior of the absorption peak as a function of the sizes of structure, pressure or aluminum concentration. This, in fact, is an expected result, taking into account the many factors that can affect both the linear and nonlinear absorption coefficients (pressure and temperature dependent dielectric constant, pressure-dependent dipole matrix element, aluminum concentration, and the dimensions of the structure).

Finally, in Fig. 9 it is shown that the total absorption coefficient dependence on the energy of the incident photon for different values of incident optical intensity. As can be noticed from the figure, the absorption coefficient decreases with the increase of intensity I and the absorption is strongly bleached at sufficiently high-incident optical intensities. Besides that, we are able to see the presence of a strong absorption saturation which begins to occur at around $I=0.7\times10^4$ W/cm^2.

4. Conclusions

In this paper we have studied the combined influence of hydrostatic pressure and aluminum concentration on the linear and nonlinear intra-band optical absorption in GaAs/$Ga_{1-x}Al_xAs$ two-dimensional concentric double quantum rings. Our results show that the behavior of the threshold energy and the position of the maximum of the intra-band optical absorption, caused by the transitions from the ground state to the first excited state,

strongly depends on the effects of hydrostatic pressure, aluminum concentration and size variation in the structure. Influence of both pressure and aluminum concentration has the consequence of a mixed resonant peak position shifting: lower hydrostatic pressure values induce a redshift whereas for high enough pressure values the peak position is shifted towards higher energies. On the contrary, augmenting the Al molar fraction in the region of smaller values of this quantity leads to a rather significant blueshift; but this change in peak position reverses towards lower energies if $x > 0.1$.

If the influence of the geometry is taken into account via the modification of the coupling barrier width, for fixed inner and outer ring dimensions, we may conclude that the increase in such a quantity induces an important redshift in the resonant peak position.

Additionally, we have found that the total optical absorption is strongly affected by the incident optical intensity and aluminum concentration. The present results can be useful in understanding the influences of hydrostatic pressure and aluminum concentration on electronic states and nonlinear optical properties in concentric double quantum rings.

Acknowledgments

C.A.D. is grateful to the Colombian Agencies CODI-Universidad de Antioquia (project: E01535-Efectos de la presión hidrostática y de los campos eléctrico y magnético sobre las propiedades ópticas no lineales de puntos, hilos y anillos cuánticos de GaAs-(Ga,Al)As y Si/SiO_2) and Facultad de Ciencias Exactas y Naturales-Universidad de Antioquia (CAD-exclusive dedication project 2012-2013). This research was partially supported by Dirección de Investigación de la Escuela de Ingeniería de Antioquia (Co-supported EIA-UdeA)-Colombia and by Armenian State Committee of Science (Project no. 11B-1c039).

References

[1] M. Tadić, F.M. Peeters, Phys. Rev. B 70 (2004) 195302.
[2] M. Tadić, F.M. Peeters, J. Phys.: Condens. Matter 16 (2004) 8633.
[3] K.L. Janssens, B. Partoens, F.M. Peeters, Phys. Rev. B 69 (2004) 235320.
[4] K.L. Janssens, B. Partoens, F.M. Peeters, Phys. Rev. B 66 (2002) 075314.
[5] K.L. Janssens, B. Partoens, F.M. Peeters, Phys. Rev. B 65 (2002) 233301.
[6] I.L. Kuskovsky, W. MacDonald, A.O. Govorov, L. Mourokh, X. Wei, M.C. Tamargo, M. Tadić, F.M. Peeters, Phys. Rev. B 76 (2007) 0353421.
[7] M.E. Mora-Ramos, A.H. Rodríguez, S.Y. López, C.A. Duque, PIERS Online 4 (2008) 263.
[8] J.M. García, G. Medeiros-Ribeiro, K. Schmidt, T. Ngo, J.L. Feng, A. Lorke, J. Kotthaus, P.M. Petroff, Appl. Phys. Lett. 71 (1997) 2014.
[9] A. Lorke, R.J. Luyken, A.O. Govorov, J.P. Kotthaus, J.M. Garcia, P.M. Petroff, Phys. Rev. Lett. 84 (2000) 2223.
[10] T. Chakraborty, P. Pietiläinen, Phys. Rev. B 50 (1994) 8460.
[11] U.F. Keyser, C. Fühner, S. Borck, R.J. Haug, M. Bichler, G. Abstreiter, W. Wegscheider, Phys. Rev. Lett. 90 (2003) 196601.
[12] S. Viefers, P. Koskinen, P.S. Deo, M. Manninen, Physica E 21 (2004) 1.
[13] P. Offermans, P.M. Koenraad, J.H. Wolter, D. Granados, J.M. García, V.M. Fomin, V.N. Gladilin, J.T. Devreese, Appl. Phys. Lett. 87 (2005) 131902.
[14] N.A.J.M. Kleemans, I.M.A. Bominaar-Silkens, V.M. Fomin, V.N. Gladilin, D. Granados, A.G. Taboada, J.M. García, P. Offermans, U. Zeitler, P.C.M. Christianen, J.C. Maan, J.T. Devreese, P.M. Koenraad, Phys. Rev. Lett. 99 (2007) 146808.
[15] L.G.G.V. Dias da Silva, J.M. Villas-Bôas, S.E. Ulloa, Phys. Rev. B 76 (2007) 155306.
[16] M. Royo, F. Malet, M. Barranco, M. Pi, J. Planelles, Phys. Rev. B 78 (2008) 165308.
[17] L.K. Castelano, G.-Q. Hai, B. Partoens, F.M. Peeters, Phys. Rev. B 78 (2008) 195315.
[18] L.K. Castelano, G.-Q. Hai, B. Partoens, F.M. Peeters, J. Appl. Phys. 106 (2009) 073702.
[19] J. Planelles, F. Rajadell, J.I. Climente, M. Royo, J.L. Movilla, J. Phys.: Conf. Ser. 61 (2007) 936.
[20] T. Chwiej, B. Szafran, Phys. Rev. B 78 (2008) 245306.
[21] T. Mano, T. Kuroda, S. Sanguinetti, T. Ochiai, T. Tateno, J. Kim, T. Noda, M. Kawabe, K. Sakoda, G. Kido, N. Koguchi, Nano Lett. 5 (2005) 425.
[22] T. Kuroda, T. Mano, T. Ochiai, S. Sanguinetti, K. Sakoda, G. Kido, N. Koguchi, Phys. Rev. B 72 (2005) 205301.
[23] M.V. Berry, Proc. R. Soc. London A 392 (1984) 45.
[24] A. Shapere, F. Wilczek, Geometric Phases in Physics; Advanced Series in Mathematical Physics, vol. 5, World Scientific Publishing Co. Inc., Singapore, 1988.
[25] J.I. Climente, J. Planelles, M. Barranco, F. Malet, M. Pi, Phys. Rev. B 73 (2006) 235327.
[26] G. Fuster, M. Pacheco, Z. Barticevic, Braz. J. Phys. 34 (2004) 666.
[27] B. Szafran, F.M. Peeters, Phys. Rev. B 72 (2005) 155316.
[28] F.J. Culchac, N. Porras-Montenegro, A. Latgé, J. Phys.: Condens. Matter 20 (2008) 285215.
[29] L. Colletti, F. Malet, M. Pi, F. Pederiva, Phys. Rev. B 79 (2009) 125315.
[30] J.M. Escartín, F. Malet, M. Barranco, M. Pi, Physica E 42 (2010) 841.
[31] J.M. Escartín, F. Malet, A. Emperador, M. Pi, Phys. Rev. B 79 (2009) 245317.
[32] J.M. Escartín, F. Malet, M. Pi, M. Barranco, Phys. Status Solidi C 7 (2010) 2608.
[33] F.J. Culchac, N. Porras-Montenegro, J.C. Granada, A. Latgé, Microelectron. J. 39 (2008) 402.
[34] V. Aroski, M. Tadić, F.M. Peeters, Acta Phys. Pol. 117 (2010) 733.
[35] F.J. Culchac, N. Porras-Montenegro, A. Latgé, J. Appl. Phys. 105 (2009) 094324.
[36] H.M. Baghramyan, M.G. Barseghyan, C.A. Duque, A.A. Kirakosyan, Proc. SPIE 8414 (2011) 84140C-1.
[37] H.M. Baghramyan, M.G. Barseghyan, C.A. Duque, A.A. Kirakosyan, J. Phys.: Conf. Ser. 350 (2012) 012016.
[38] E.M. Goldys, J.-J. Shi, Phys. Status Solidi B 210 (1998) 237.
[39] D. Ahn, S.-L. Chuang, IEEE J. Quantum Electron. 23 (1987) 2196.
[40] R.F. Kazarinov, R.A. Suris, Sov. Phys. Semicond. 5 (1971) 707.
[41] D.A.B. Miller, Int. J. High Speed Electron. Syst. 1 (1990) 19.
[42] T.H. Hood, J. Lightwave Technol. 6 (1988) 743.
[43] H. Yildirim, M. Tomak, Eur. Phys. J. B 50 (2006) 559.
[44] I. Karabulut, S. Baskoutas, J. Appl. Phys. 103 (2008) 073512.
[45] W.F. Xie, Phys. Lett. A 372 (2008) 5498.
[46] Jian-Hui Yuan, Jin-Sheng Huang, Miao Yin, Qi-Jun Zeng, Jun-Pei Zhang, Opt. Commun. 283 (2010) 3529.
[47] W.F. Xie, Phys. Lett. A 374 (2010) 1188.
[48] Shijun Liang, W.F. Xie, H.A. Sarkisyan, A.V. Meliksetyan, H. Shen, J. Phys.: Condens. Matter 23 (2011) 415302.
[49] C.M. Duque, M.E. Mora-Ramos, C.A. Duque, Physica E 43 (2011) 1002.
[50] I. Karabulut, M.E. Mora-Ramos, C.A. Duque, J. Lumin. 131 (2011) 1502.
[51] M.G. Barseghyan, A.A. Kirakosyan, C.A. Duque, Eur. Phys. J. B 72 (2009) 521.
[52] M.G. Barseghyan, M.E. Mora-Ramos, C.A. Duque, Eur. Phys. J. B 84 (2011) 265.
[53] E. Reyes-Gómez, N. Raigoza, L.E. Oliveira, Phys. Rev. B 77 (2008) 115308.
[54] A.M. Elabsy, J. Phys.: Condens. Matter 6 (1994) 10025.
[55] A. Wojs, P. Hawrylak, S. Farard, L. Jacak, Phys. Rev. B 54 (1996) 5604.
[56] R.W. Boyd, Nonlinear Optics, Academic Press, San Diego, 2003.